Lattice-Boltzmann simulation of two-dimensional flow over two vibrating side-by-side circular cylinders

Yousheng Xu,[1,2,*] Yang Liu,[2] Yong Xia,[1,2] and Fengmin Wu[1]
[1]*Department of Physics, Zhejiang Normal University, Jinhua, Zhejiang 312004, China*
[2]*Department of Mechanical Engineering, The Hong Kong Polytechnic University, Kowloon, Hong Kong, China*
(Received 3 January 2008; revised manuscript received 24 July 2008; published 27 October 2008)

A numerical simulation using the multiple relaxation time lattice-Boltzmann method is carried out for the purpose of investigating fluid flow over two vibrating side-by-side circular cylinders and the effect of moving the cylinders on the wake characteristics. As a benchmark problem to assess the validity and efficiency of the model, the calculation was carried out at Reynolds number of 200 and four pitch ratios (T/D, where D is the cylinder diameter while T is the center-to-center spacing between the two cylinders) of 1.2, 1.6, 2.2, and 3.2, respectively. The calculated results indicate that the vibration of the cylinder pair has significant influence on the wake patterns. When the amplitude of vibration is big enough, the vibration locks up the vortex shedding and formation. For each cylinder vibration frequency, there exists a threshold of vibration amplitude for the lock-up phenomenon. With the vibration frequency is increased, the threshold of vibration amplitude decreases.

DOI: 10.1103/PhysRevE.78.046314 PACS number(s): 47.32.−y, 47.10.−g, 47.11.−j

I. INTRODUCTION

Complex wakes behind a single or multiple circular cylinders have attracted a great deal of research experimentally and, more recently, numerically, due to their academic and engineering importance [1–5]. So far, flow over a single circular cylinder has been used just as a building-block problem for understanding the vortex dynamics and controlling vortex shedding in a bluff-body wake. Therefore, much research has been performed on single-cylinder flow. However, as reported by Jester and Kallinderis [6], many engineering structures involve multiple bluff bodies in proximity. Depending on the configuration of these bodies relative to the flow, a wide variety of interference phenomena can be observed. Even the simplest case of two identical circular cylinders presents a rich spectrum of different flow features.

The present study numerically investigates one of the simplest complex-geometry flows, that is, flow over two identical circular cylinders in a side-by-side arrangement, which is found in many applications such as tube bundles in heat exchangers, fuel and control rods in nuclear reactors, piers and bridge pilings, oil and gas pipelines, cooling-tower arrays, suspension bridges, and high-rise buildings. The flow field of two finite cylinders is strongly influenced by the cylinders' pitch ratios (T/D, where D is the cylinder diameter while T is the center-to-center spacing between the two cylinders). When two finite circular cylinders are arranged in a staggered configuration, the interaction between the downwash flows from the two cylinders, along with the strong flow interference happening at the bases of the two cylinders, makes the flow pattern even more complex and challenging to study. Most of the previous work on the flow around two staggered finite circular cylinder has been focused on measurements of the mean pressure distributions and aerodynamic forces.

Numerous experimental studies have been performed on the flow around two side-by-side cylinders set normal to the free stream. Spivack [7] investigated the predominant frequencies in the flow field behind a pair of cylinders using a hot wire technique over a Reynolds number range of 1.5×10^4–9.3×10^4, and discovered three distinct regimes of flow with different spacing ratios T/D. Bearman and Wadcock [8] suggested that the repulsive forces acting between two circular cylinders originated from a rotation of the resultant force created by the presence of the neighboring cylinder. They also found that the asymmetry was due to a near-wake phenomenon and not to the position of the boundary layer separation. On the other hand, Williamson [9] found the existence of harmonic vortex-shedding modes behind a pair of cylinders, and observed that the shedding frequency on one side of the wake was a multiple of that on the other. Sumner *et al.* [10] studied the fluid-structure interaction phenomenon in a water tunnel. They found that the reported bistable nature of the biased flow was not detected in the water tunnel experiments. Consequently, they questioned whether this was a coincidence or whether there was a deeper underlying reason.

Compared to experimental studies, there have been relatively few numerical investigations of the flow around two circular cylinders. Stansby [11] used an essentially inviscid discrete-vortex method to investigate two side-by-side cylinders in a cross flow and was able to reproduce most of the gross wake features observed experimentally. Chang and Song [12] simulated the flow around two side-by-side circular cylinders at Re=100 for $T/D=1.7$ and 3.0. They used a blended technique, which was made up of a finite-element method for the vicinity of the circular cylinders and a finite-difference method for the rest of the flow field, to tackle the problem. Flow visualization and force coefficients were shown to agree well with experimental data. Mittal *et al.* [13] used a stabilized finite element method to simulate three configurations at Re=100 and 1000. Again, good agreement with measured results was obtained. Furthermore, their results showed that Re=100 flow was sufficient to reproduce flow features observed in experimental results gathered at a much higher Reynolds number. Schulz and Kallinderis [14]

*mmyliu@polyu.edu.hk; ysyou@zjnu.cn

used a finite-volume method to compute the flow and structural response for a pair cylinders at Re=110. Their studies proved that the vortices obtained from two parallel circular cylinders could interfere with each other and generate a biased flow pattern which affects the flow-induced forces; moreover, this biased flow pattern switches intermittently from being directed towards one cylinder to the other, and the flow pattern is termed bistable. Tezduyar *et al.* [15] used a finite-element formulation with the streamline-upwind Petrov-Galerkin method to investigate a similar problem with $T/D=1.5$ and Re=100. On the other hand, Slaouti and Stansby [16] studied the flow around two side-by-side circular cylinders using the random-vortex method. Their calculations were carried out at Re=200 and several T/D ratios. Most of the numerical investigations considered rigid cylinders only, where the cylinders are assumed to have infinite structural stiffness. Consequently, the interactions between the fluid and the elastic structures were not investigated.

Actually, the wake patterns behind two side-by-side circular cylinder are approximately categorized into three primary flow regimes [17]. The first is single body ($T/D \leqslant 1.2$), similar to the tandem case, when the cylinders are placed side-by-side in extremely close proximity, they behave as a single body with a single vortex street. The second is biased gap ($1.2 < T/D < 2.0$), where for intermediate spacings, the flow in the gap between the cylinders is deflected toward one of the cylinders. Thus, two distinctive near wakes are formed, one wide and one narrow. The particular direction of the bias will intermittently change, indicating another bistable state. The last is coupled vortex streets ($2.0 \leqslant T/D \leqslant 4.0$). In this region, two distinct vortex streets are formed. These vortex streets are usually coupled in a symmetric manner, i.e., vortices are alternatively shed on the gap side and then the outside of the cylinders.

To our knowledge, the physical nature of the transition to two-dimensional (2D) wake is one of the most basic and revealing cases in the general subject of circular cylinder-body flow. On the other hand, simulations of the corresponding 2D flow around a long slender cylinder and the associated flow-induced forces have been amply carried out [18]. Most of the numerical simulations rely on a continuum model described by the Navier-Stokes equations. These simulations provide valuable time series for the mean and fluctuating forces and for the velocity field in the wake flow. Most of the 3D numerical studies invoked periodic boundary conditions at both ends of the cylinder, thus tacitly assuming the spanwise variations to have a certain period that is specified *a priori*. These studies could provide an approximate model for the midspan wake flow, but fail to take the end effects into account. Only very few calculations have attempted to consider the effect of the end walls on the wake flow. Direct numerical simulation employing a spectral method was used to calculate the wake flow and the unsteady forces acting on a stationary rigid cylinder assuming periodic boundary conditions [19]. Again, only results at midspan were given and no spanwise variation of the unsteady forces was reported. In all these calculations, the flow-induced forces were tacitly assumed to be stationary after the transient period has elapsed. Therefore, these data are inappropriate to use to carry out an investigation of wake effects on the behavior of the flow-induced forces, if any.

In most cases presented in the literature, the Reynolds number is large and the flows are transitional or turbulent. Because of this, many of the flow features have a complex structural nature. These characteristics make numerical analysis difficult, even using direct numerical simulation of the governing Navier-Stokes equations [20]. Therefore, it is necessary to develop powerful numerical methods to treat such problems. Recently, a different numerical simulation method, the lattice-Boltzmann method (LBM) has been used frequently [21–24] because of its advantages of easy programming and good parallelism to directly solve various fluid problems. In particular, many LBM simulations were done on the problem of cylinders in a cross flow [5,14,25–28]. As described earlier in these papers, all the work employed the Bhatnagar-Gross-Krook collision operator for which every variable relaxes toward equilibrium with the same time scale τ; this is termed the single relaxation time (SRT) method. But Luo and Lallemand found that the SRT is not stable enough in some complicated cases [23], and they proposed using a more complicated collision operator for which each variable relaxes toward equilibrium with different time scales τ_i. This is the multiple relaxation time (MRT) collision operator. Recently, our team carried out several studies on cylinder wakes [29–33]. In these studies, the cylinders were rigid and the flow was three dimensional. Now we extend our study to the effect of a moving boundary on cylinder wakes using MRTLBM.

The main objective of the present paper is to investigate the two-dimensional wake interference behind a vibrating side-by-side cylinder pair in a cross flow. The MRTLBM and two-dimensional nine-velocity (D2Q9) model are selected. The parallel cylinder pair vibrate periodically and synchronously, and a moving boundary condition is used. The calculation is carried out at $T/D=1.2, 1.6, 2.2, 3.2$, respectively, and Re=200.

The rest of this paper is organized as follows. In Sec. II, the numerical model and method are briefly described, and in Sec. III, the treatment of the moving boundary of the cylinders is demonstrated. Section IV shows numerical results and the analysis, and then come the conclusions in Sec. V.

II. NUMERICAL METHOD

A. Problem description

A schematic view is illustrated in Fig. 1. The two side-by-side circular cylinders, bounded by a rectangular computational domain in which the width is $H/D=16$ and the length is $L/D=24-40$ are exposed to a cross flow, and the two cylinders are vibrating along the x axis synchronously and periodically at the amplitude $A/D=0.2-1.0$ and the frequency 0.2–0.6. The two circular cylinders are identical, with diameter D. Incompressible flow with constant fluid density ρ and dynamic viscosity μ is assumed. A Cartesian coordinate system (x,y), where the x *axis* is aligned with the streamwise direction, is used to describe the flow. All physical parameters are normalized by D, ρ, μ, and U_∞. The normalized flow-induced force coefficient acting on the cylinder axis is decomposed into a drag coefficient $C_d(t)$ and a lift

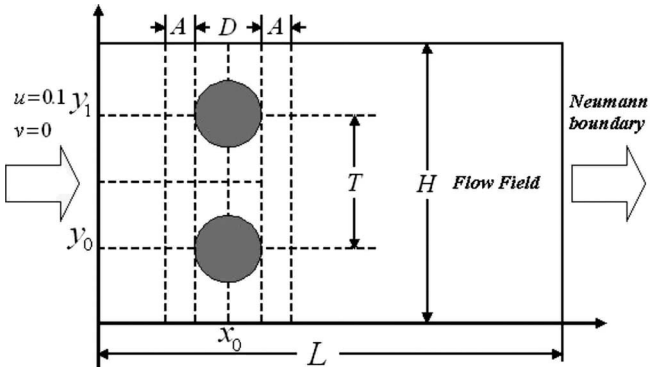

FIG. 1. Schematic view of the problem: T is the center-to-center distance of two cylinders; D is the diameter; H and L are the width and length of the flow field, respectively; A is the vibration amplitude of the two cylinders.

coefficient $C_l(t)$, where the nondimensional time is defined as $t=\tilde{t}U_\infty/D$ and the nondimensional coordinates are denoted by capital letters. Here, the tilde is used to denote dimensional quantities. A lattice-Boltzmann method with multiple relaxation times is used to solve the flow field numerically. In the simulation, the boundary conditions are given as follows: at the inlet, the velocity is uniform, i.e., $u=0.1$; at the outlet, Neumann conditions are used; on the surface of the moving cylinders, the no-slip condition is applied and the bounce-back boundary condition and the interpolation are implemented. In the flow field, we tested two different lattice cases: one has 24 lattices in one diameter and the other 32. The results for the mean values of the drag and lift on the cylinder showed that the discrepancies of these mean forces between this two settings are below 5%. So the setting of 24 lattices in one diameter is accurate enough.

B. Multiple relaxation time lattice Boltzmann method

A D2Q9 model is adopted in the calculation. The Boltzmann equation is formulated based on the one-body distribution function $f(\mathbf{x},\mathbf{e},t)$, which is the density of molecules at position $\mathbf{x}$ and speed $\mathbf{e}$ at time t, so macroscopic variables like the fluid density ρ and velocity $\mathbf{u}$ are expressed as moments of a discrete set of $f(\mathbf{x},\mathbf{e},t)$,

$$\rho = \sum f_i, \quad \rho\mathbf{u} = \sum \mathbf{e}_i f_i, \tag{1}$$

where $\mathbf{e}_i$ is the particle speed, and f can be written in its nondimensional form as

$$\frac{\partial f}{\partial t} + \mathbf{e}\cdot\nabla f = G(f,f), \tag{2}$$

where the terms on the left side of Eq. (2) describe the free streaming of molecules in space, and the term $G(f,f)$ on the right side of Eq. (2) represents a complicated integral operator in the velocity field expressing intermolecular interactions or collisions. In the MRT method, the collision operator $G(f,f)$ makes variables relax toward equilibria with different time scales. The MRT model [34] is implemented in this study. The lattice Boltzmann equation (LBE) can be written as

$$f(\mathbf{r}_i + \mathbf{e}_\alpha\delta t, t+\delta t) = f(\mathbf{r}_i,t) - \mathbf{S}[|f(\mathbf{r}_i,t)\rangle - f^{\mathrm{eq}}(\mathbf{r}_i,t)], \tag{3}$$

where

$$f(\mathbf{r}_i,t) \equiv (f_0(\mathbf{r}_i,t), f_1(\mathbf{r}_i,t), \ldots, f_N(\mathbf{r}_i,t))^T, \tag{4}$$

$$f_i^{\mathrm{eq}} = w_i\rho\left(1 + 3\mathbf{e}_i\cdot\mathbf{u} + \frac{9}{2}(\mathbf{e}_i\cdot\mathbf{u})^2 - \frac{3}{2}\mathbf{u}^2\right). \tag{5}$$

With MRTs, Eq. (3) becomes [23,34]

$$f(\mathbf{r}_i + \mathbf{e}_\alpha\delta t, t+\delta t) - f(\mathbf{r}_i,t) = -M^{-1}\hat{S}[m(\mathbf{r}_i,t) - m^{\mathrm{eq}}(\mathbf{r}_i,t)], \tag{6}$$

where m is the moment, m^{eq} is the equilibrium value of the moment, M is the transformation matrix, $m=Mf$, and $f=M^{-1}m$. Following the method of Ginzburg [35], the transformation matrix M of the incompressible MRTLBM is obtained:

$$M = [|p\rangle, |e\rangle, |e^2\rangle, |u_x\rangle, |q_x\rangle, |u_y\rangle, |q_y\rangle, |p_{xx}\rangle, |p_{xy}\rangle]^T. \tag{7}$$

The corresponding equilibrium distribution functions in moment space, m^{eq}, are given by

$$m = [\rho_0, e^{\mathrm{eq}}, e^{2\mathrm{eq}}, u_x, q_x^{\mathrm{eq}}, u_y, q_y, p_{xx}^{\mathrm{eq}}, p_{xy}^{\mathrm{eq}}]^T. \tag{8}$$

The collision matrix $\hat{\mathbf{S}}=M^{-1}SM$ is

$$\hat{\mathbf{S}} = \mathrm{diag}\{0, s_1, s_2, 0, s_4, 0, s_6, s_7, s_8\}, \tag{9}$$

where $s_1=1.63$, $s_2=1.14$, $s_4=s_6=1.92$, and

$$\nu = \frac{1}{3}\left(\frac{1}{s_7} - \frac{1}{2}\right) = \frac{1}{3}\left(\frac{1}{s_8} - \frac{1}{2}\right), \tag{10}$$

i.e., $s_7=s_8=1/(3\nu+0.5)$, where ν is the viscosity determined by the Reynolds number.

In the works of Lallemand and Luo [23] and d'Humières *et al.* [36], the dispersion, dissipation, isotropy, Galilean invariance, and stability of the LBM are discussed thoroughly. With the optimized parameters given in those papers, the hydrodynamics regime, impressibility, and stability can be ensured when $\mathbf{u}$ and ν vary within specified limits. In our simulation, $u=0.1$ and $\nu=4\times10^{-3}$, which satisfy this requirement.

III. BOUNDARY CONDITIONS

For the LBM, there have been several models to tackle the moving boundary problem, particularly the treatment for a curved boundary. The treatment for a curved boundary is a combination of the bounceback scheme and interpolations. Lallemand and Luo [37] made a simple modification to this treatment, which is illustrated in Fig. 2.

In this study, we follow the method of Lallemand and Luo [37]. When the cylinders are vibrating, the following interpolation formulas (where the notations $\hat{f}_\alpha$ and f_α denote the postcollision distribution functions before and after advection) are used:

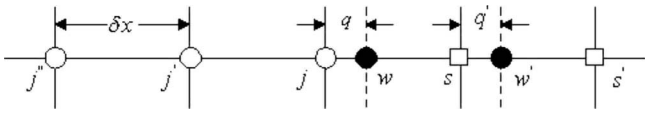

FIG. 2. Illustration of boundary scheme. Empty circles are the fluid nodes, and empty squares are the solid nodes. Dark disks are the boundary-located nodes. The thin solid lines are the grid lines, the dashed lines are the boundary locations situated arbitrarily between two grids, and the boundary moves from w at time t to w' after a time step, so node s becomes a fluid instead of a solid node.

$$f_{\bar{\alpha}}(\mathbf{r}_j,t) = q(1+2q)\hat{f}_{\alpha}(\mathbf{r}_j,t) + (1-4q^2)\hat{f}_{\alpha}(\mathbf{r}_{j'},t) + q(1-2q)\hat{f}_{\alpha}(\mathbf{r}_{j''},t) + 3w_{\alpha}(\mathbf{e}_{\alpha}\cdot\mathbf{u}_w), \quad q<1/2, \tag{11}$$

$$f_{\bar{\alpha}}(\mathbf{r}_j,t) = \frac{1}{q(2q+1)}\hat{f}_{\alpha}(\mathbf{r}_j,t) + \frac{(2q-1)}{q}f_{\bar{\alpha}}(\mathbf{r}_{j'},t) - \frac{2q-1}{2q+1}f_{\bar{\alpha}}(\mathbf{r}_{j''},t) + \frac{3w_{\alpha}}{q(2q+1)}(\mathbf{e}_{\alpha}\cdot\mathbf{u}_w), \quad q\geqslant 1/2, \tag{12}$$

where $f_{\bar{\alpha}}$ is the distribution function of the velocity $\mathbf{e}_{\bar{\alpha}}\equiv-\mathbf{e}_{\alpha}$, and $\mathbf{u}_w$ is the velocity of the moving wall at the point $\mathbf{r}_w$ in Fig. 2. The term in proportion to $w_{\alpha}(\mathbf{e}_{\alpha}\cdot\mathbf{u}_w)$ is the momentum exerted on the fluid by the moving wall of velocity $\mathbf{u}_w$. Suppose a forcing term F is introduced due to the fluid-wall interaction, then the mass conservation $\Sigma_{\alpha}F_{\alpha}=0$ and the momentum conservation $\Sigma_{\alpha}\mathbf{e}_{\alpha}F_{\alpha}=\rho_0\mathbf{u}_w$ immediately lead to $F_{\alpha}=3w_{\alpha}(\mathbf{e}_{\alpha}\cdot\mathbf{u}_w)$ [38,39].

In practice, by combining collision and advection into one step, the actual formulas used in simulations are

$$f_{\bar{\alpha}}(\mathbf{r}_j,t) = q(1+2q)f_{\alpha}(\mathbf{r}_j+\mathbf{e}_{\alpha}\delta_t,t) + (1-4q^2)f_{\alpha}(\mathbf{r}_j,t) - q(1-2q)f_{\alpha}(\mathbf{r}_j-\mathbf{e}_{\alpha}\delta_t,t) + 3w_{\alpha}(\mathbf{e}_{\alpha}\cdot\mathbf{u}_w), \quad q<\frac{1}{2}, \tag{13}$$

$$f_{\bar{\alpha}}(\mathbf{r}_j,t) = \frac{1}{q(2q+1)}f_{\alpha}(\mathbf{r}_j+\mathbf{e}_{\alpha}\delta_t,t) + \frac{(2q-1)}{q}f_{\bar{\alpha}}(\mathbf{r}_j-\mathbf{e}_{\alpha}\delta_t,t) - \frac{2q-1}{2q+1}f_{\bar{\alpha}}(\mathbf{r}_j-2\mathbf{e}_{\alpha}\delta_t,t) + \frac{3w_{\alpha}}{q(2q+1)}(\mathbf{e}_{\alpha}\cdot\mathbf{u}_w), \quad q\geqslant\frac{1}{2}. \tag{14}$$

The above formulas are implemented as follows.

Suppose the vibrating velocity of cylinder is $\mathbf{u}_w$, as shown in Fig. 2; when a grid point s moves from the nonfluid region into the fluid region, the unknown distribution functions $f_{\alpha}(\mathbf{r}_s)$ on this node have to be specified. We use a second-order extrapolation to compute the unknown distribution functions along the direction of a chosen discrete velocity $\mathbf{e}_{\alpha}$ which maximizes the quantity $\hat{\mathbf{n}}\cdot\mathbf{e}_{\alpha}$, where $\hat{\mathbf{n}}$ is the out-normal vector of the wall at the point through which the node moves to the fluid region. For example, the unknown distribution functions $f_{\alpha}(\mathbf{r}_s)$ at node s as depicted in Fig. 2 is given by the following extrapolation formula:

$$f_{\alpha}(\mathbf{r}_s) = 3f_{\alpha}(\mathbf{r}_j) - 3f_{\alpha}(\mathbf{r}_j') + f_{\alpha}(\mathbf{r}_j''+\mathbf{e}_{\alpha}). \tag{15}$$

Obviously, the method used to compute values of the unknown distribution functions (on the nodes which move from the nonfluid to the fluid region) is not unique. One could choose any similar method and get similar results.

To study the induced force on the cylinders, we have to get the momentum transfer occurring on the boundaries of cylinders. The momentum transfer $\mathbf{\Phi}$ along the direction of $\mathbf{e}_{\alpha}$ is equal to

$$\mathbf{\Phi}_{\alpha} = \mathbf{e}_{\alpha}[f_{\alpha}(\mathbf{r}_w,t) + \mathbf{f}_{\bar{\alpha}}(\mathbf{r}_w,t)]. \tag{16}$$

The above formula gives the momentum flux through any boundary normal to $\mathbf{e}_{\alpha}$ located at boundary point $\mathbf{r}_w$ or $\mathbf{r}_w'$ in Fig. 2. In the simulations, we use the above formula to evaluate momentum exchange in the interaction between the fluid and the solid bodies.

TABLE I. Comparison of the mean drag and lift coefficients between Meneghini *et al.* [4] and present study.

T/D	$\bar{C}_{d1}$	$\bar{C}_{d2}$	$\bar{C}_{l1}$	$\bar{C}_{l2}$
Meneghini *et al.* [4]				
1.5D	1.32	1.32	−0.40	0.40
2D	1.42	1.42	−0.22	0.22
3D	1.41	1.41	−0.10	0.10
4D	1.34	1.34	−0.05	0.05
Present study				
1.5D	1.31	1.31	−0.39	0.38
2D	1.43	1.43	−0.23	0.23
3D	1.41	1.41	−0.09	0.09
4D	1.32	1.32	−0.05	0.05

IV. RESULTS AND DISCUSSION

The computational code for the three-dimensional case was validated against measurements and other calculations elsewhere [33]; the interested reader can refer to that paper. To further validate the credibility of our code in 2D domain, we compare the mean force on two side-by-side rigid cylinders in a cross flow at Re=200 and T/D=1.5,2.0,3.0,4.0 with those of Meneghini *et al.* [4]. The current calculated mean drag and mean lift and the data of Meneghini *et al.* are tabulated in Table I. The agreement is good, and the largest discrepancy is about 4%.

Having validated the MRTLBM for a 2D rigid cylinder calculation, the next step is to assess the effect of cylinder vibrations on the wake flow and, in turn, the influences of the wake flow on the flow-induced forces. Here, how cylinder

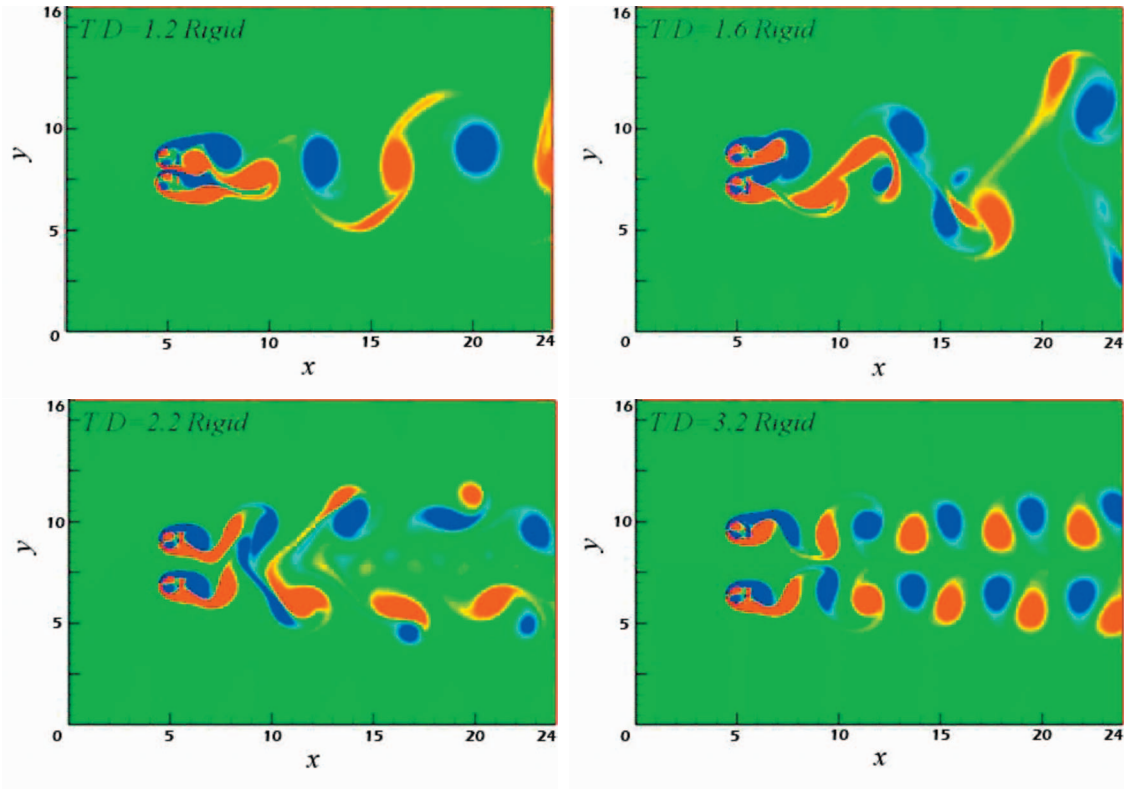

FIG. 3. (Color) Rigid cylinder pair vortex formation at Re=200: $T/D=1.2$, 1.6, 2.2, and 3.2. The green bottom denotes the flow field; the red denote clockwise and blue counterclockwise vortices, in this and the following figures.

vibrations would modify this effect is examined in detail by comparing the rigid and vibrating cases. The calculations were carried out for both rigid and vibrating cases at $T/D=1.2$, 1.6, 2.2, and 3.2, respectively. Since the vortex shedding frequency of these cylinder arrangements is about 0.1 and 0.2, respectively, we choose the representative cylinder vibration frequency as 0.4 which is the harmonic of the Strohal number and could produce the vortex lock-up phenomenon easily [40]. Later, we will also examine the effect of vibration frequency on the vortex lock-up phenomenon with vibration frequencies of 0.2–0.6. The vibration amplitude is set as $A/D=0.2$, 0.3, 0.4, 0.5, and 1.0, respectively.

Figure 3 shows the vortex patterns of rigid cylinders at different spacing ratios. Vortex formation shows that the cylinder pair at $T/D=1.2$ behaves like a single bluff body; in one cycle two vortices are released, one from the bottom and

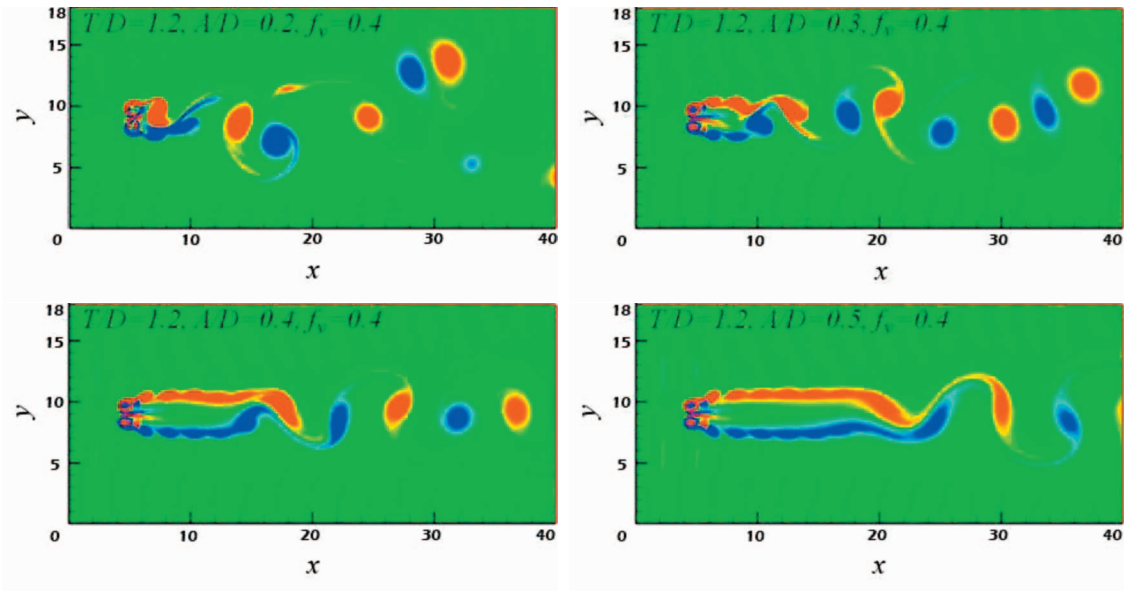

FIG. 4. (Color) Vibrating cylinder pair vortex formation at $T/D=1.2$ and different vibration amplitudes.

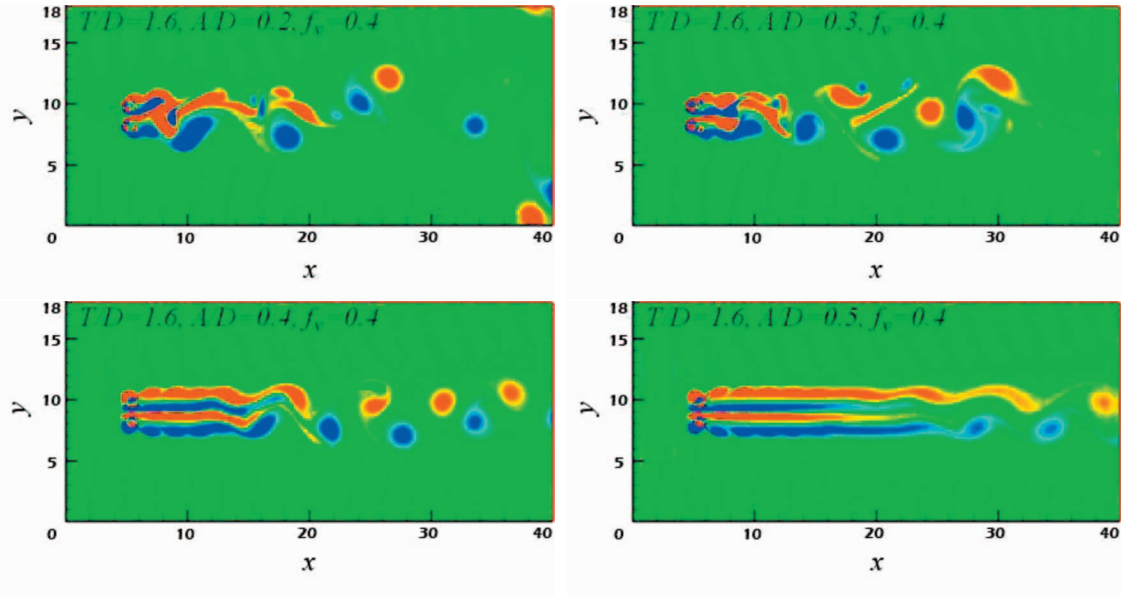

FIG. 5. (Color) Vibrating cylinder pair vortex formation at $T/D=1.6$ and different vibration amplitudes.

the other from the top, and they are aligned behind the cylinder pair. For $T/D=1.6$ and 2.2, the predominant wake pattern observed is the deflected wake pattern. According to Williamson [9], for Re=200, there are two types of basic behavior in the vortex dynamics of the combined wake for a biased flow pattern. In the first case, vortices formed alongside the biased gap flow are squeezed and amalgamated into dominant vortices on the outside of the two-cylinder configuration, the side to which the flow is biased. This amalgamation process eventually produces a single vortex street in the combined wake. In the present calculation, the figure of $T/D=1.6$ exactly shows the simulation of this phenom-

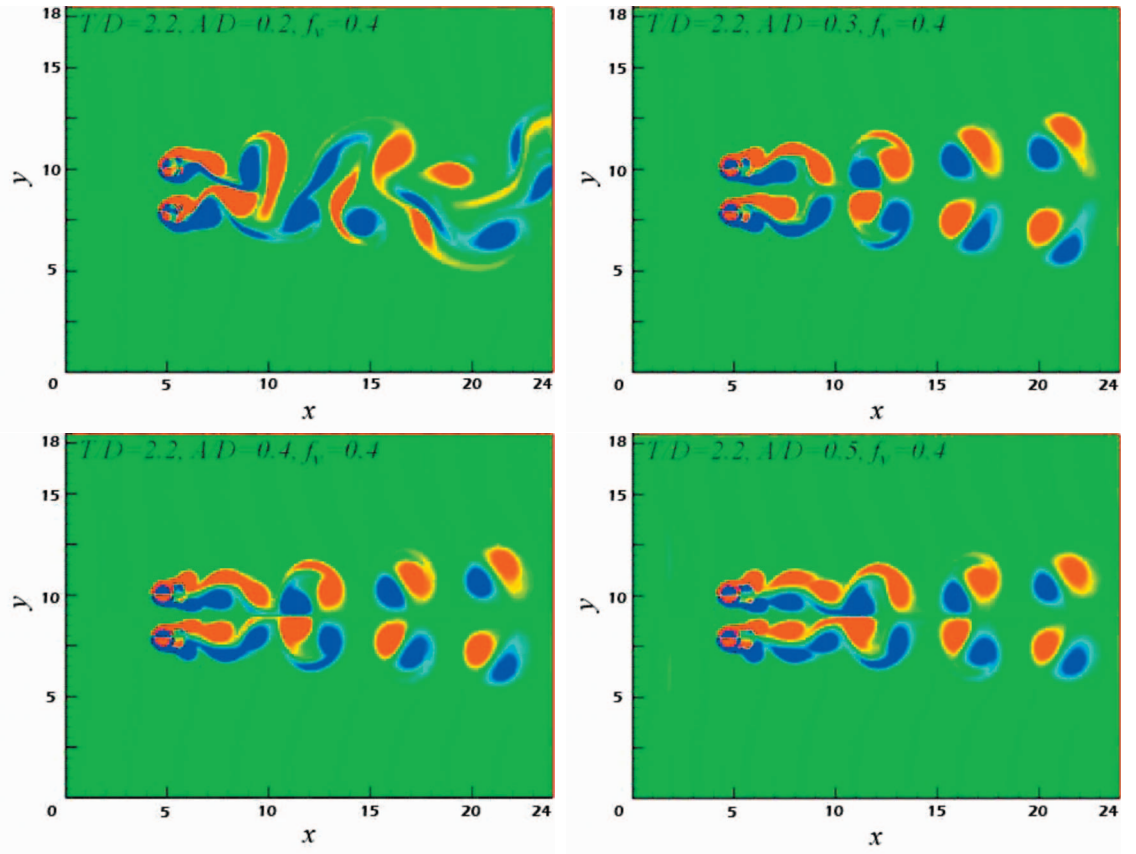

FIG. 6. (Color) Vibrating cylinder pair vortex formation at $T/D=2.2$ and different vibration amplitudes.

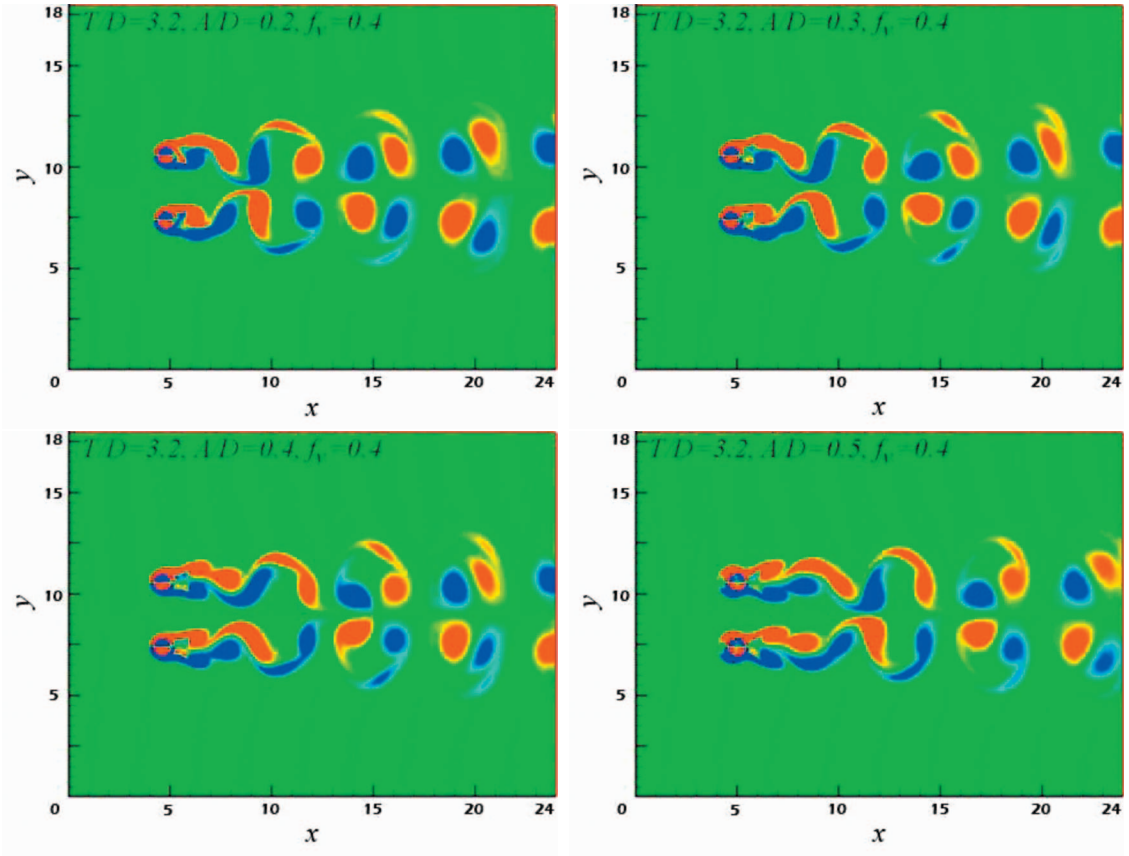

FIG. 7. (Color) Vibrating cylinder pair vortex formation at $T/D=3.2$ and different vibration amplitudes.

enon. In the second case of Williamson, the combined wake of the two cylinders is marked by pairs of vortices downstream of the cylinder with a narrow near-wake region, and single larger vortices downstream of the cylinder with a wider near-wake region, on the opposite side. In this case, the gap vortices are amalgamated into the side of the wake where the pairs form. For $T/D=3.2$, the interaction of the two cylinders is weak, and the vortex shedding from the two cylinders is antiphase. This leads to the formation of a single, binary vortex street in the combined wake of the two cylinders.

Figure 4 shows the effect of vibration amplitude on vortex formation at vibration frequency $f_v=0.4$ for $T/D=1.2$. To properly count the vortex formation behind the cylinder pair, the downstream domain is extended to $40D$. For vibration amplitude $A/D=0.2$, the vortex shedding pattern behind the vibrating cylinder pair is slightly modified; the spacing between the vortices is no longer equal but exhibits alternately a long short pattern due to the streamwise motion of the cylinder pair. Moreover, the vortex street seems to oscillate in the transverse direction. At $A/D=0.3$, the cylinder vibration speed is faster, and this vibration seems to lock up the vortex formation. In one cycle, two small vortices are released almost simultaneously from both top and bottom of the pair; these two vortices superpose on the vortices released in the previous cycle to form two parallel connected vortex streets. After these two parallel connected vortex streets, a larger alternative vortex is formed that exhibits the typical Karmon vortex street. Also, the alternately long-short pattern is observed due to the streamwise motion of the cylinder pair. With increasing vibration amplitude ($A/D=0.4$ and 0.5), the parallel connected vortex street becomes longer, the spacing between the vortices is uniform, and the long-short pattern disappears.

Figure 5 shows the vortex formation at $f_v=0.4$ for $T/D=1.6$ with different vibration amplitude. Again, the downstream domain is extended to $40D$, which allows the vortices to develop thoroughly. At $A/D=0.2$ and 0.3, there is no major change in the wake behind the vibrating cylinder pair compared to the rigid case. When the vibration amplitude is increased to $A/D=0.4$, and 0.5, the vibration regulates the vortex shedding, four parallel connected vortex streets are formed, and then these small vortices evolve into a Karmon vortex street. With larger vibration amplitude, the four parallel connected vortex streets are longer, and the vortex formation is more regular.

Figure 6 shows the vortex formation at $f_v=0.4$ for $T/D=2.2$ with different vibration amplitudes. At $A/D=0.2$, there is almost no discernible change in the vortex formation. When the amplitude is increased to $A/D=0.3-0.5$, the vortex shedding is regulated by the vibration to a long-short pattern, and the interaction between the two cylinders becomes weak. Figure 7 shows the vortex formation at $f_v=0.4$ for $T/D=3.2$ with different vibration amplitude. At this spacing ratio, the interaction of the two cylinders is weak, and the vortex shedding from the two cylinders is antiphase. This leads to the formation of a single, binary vortex street in the combined wake of the two cylinders. The vibration modi-

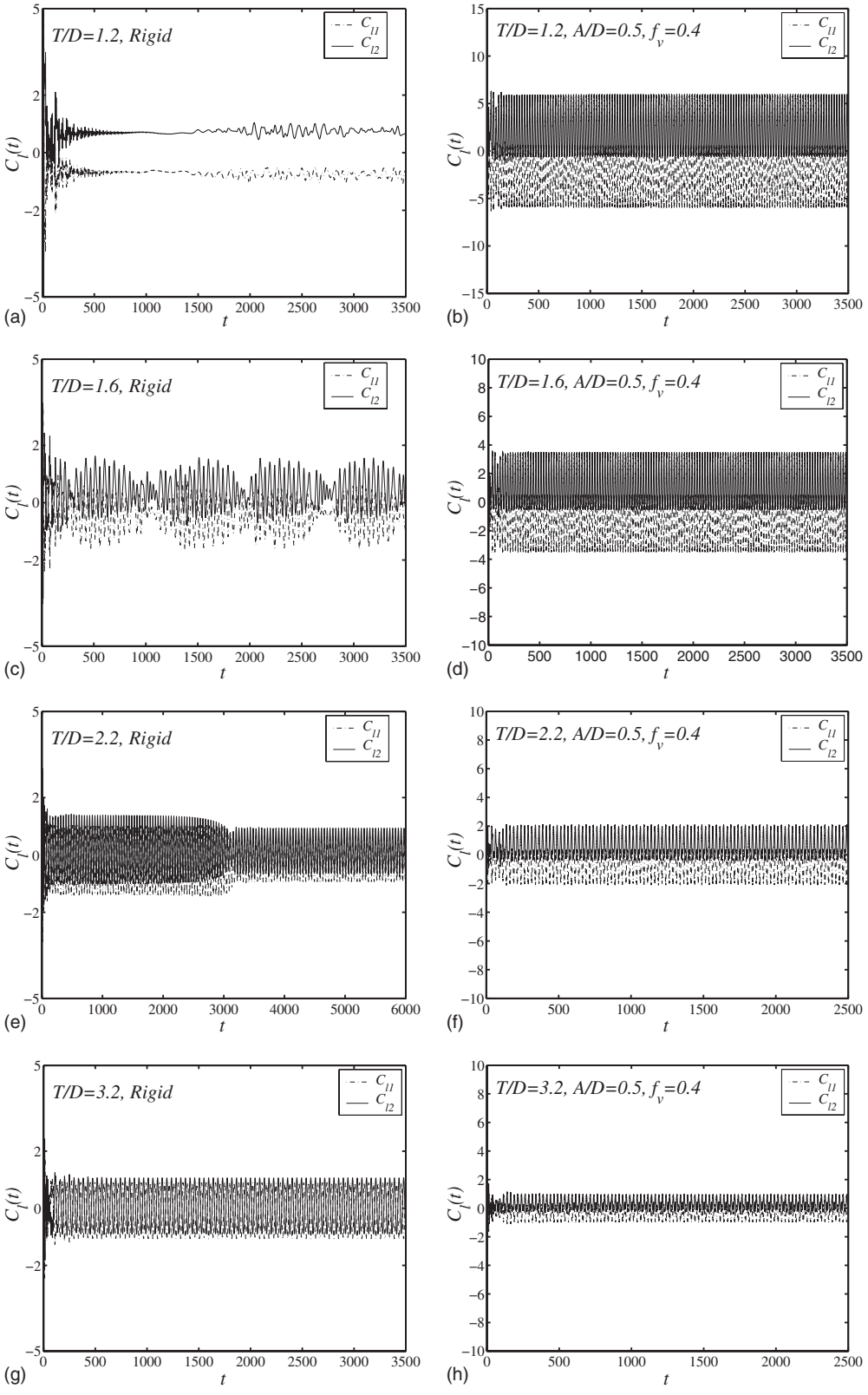

FIG. 8. Lift time series at different spacing ratios for rigid and vibrating cylinders at $A/D=0.5$.

fied the vortex formation slightly, the spacing between vortex is lengthened and exhibits an alternately long-short pattern due to the streamwise vibration of the cylinders.

Figure 8 shows the lift time series at different spacing ratios for rigid and vibrating cylinders at $A/D=0.5$. At $T/D=1.2$, the vibration enhances and regulates the vortex shedding; consequently, the lift time series exhibits a much larger and regular pattern. At $T/D=1.6$, there exists a beating phenomenon for the rigid case; however, for the vibrating case, the vibration regulates the series and eliminates the beating phenomenon. At $T/D=2.2$ and 3.2, the vibration enhances the vortex shedding and increases the lift amplitude.

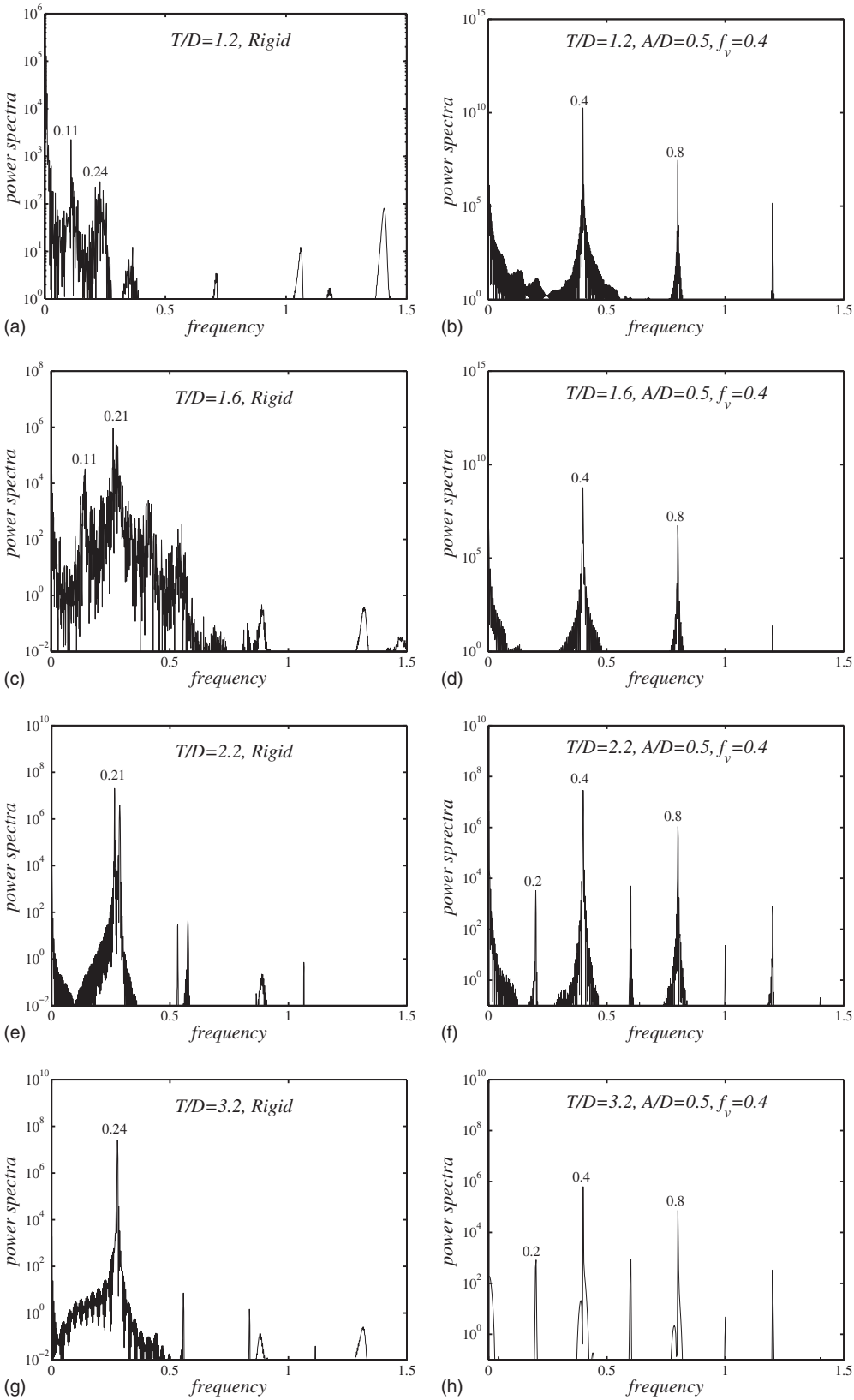

FIG. 9. Lift power spectral analysis for both rigid and vibrating cylinders at $A/D=0.5$.

Figure 9 shows the lift power spectrum at different spacing ratios for both rigid and vibration cylinders at $A/D=0.5$. The cylinder vibration has a significant influence on the vortex shedding frequency. For the rigid case, the shedding frequency is about 0.1 at $T/D=1.2$; but for the vibrating case, the vortex shedding is locked up by the cylinder vibration and the shedding frequency becomes 0.4. The same phenomena can be found at the other three spacing ratios; it is obviously that the vortex shedding is locked by the cylinder vibration ($f_v=0.4$), and the dominant vortex shedding fre-

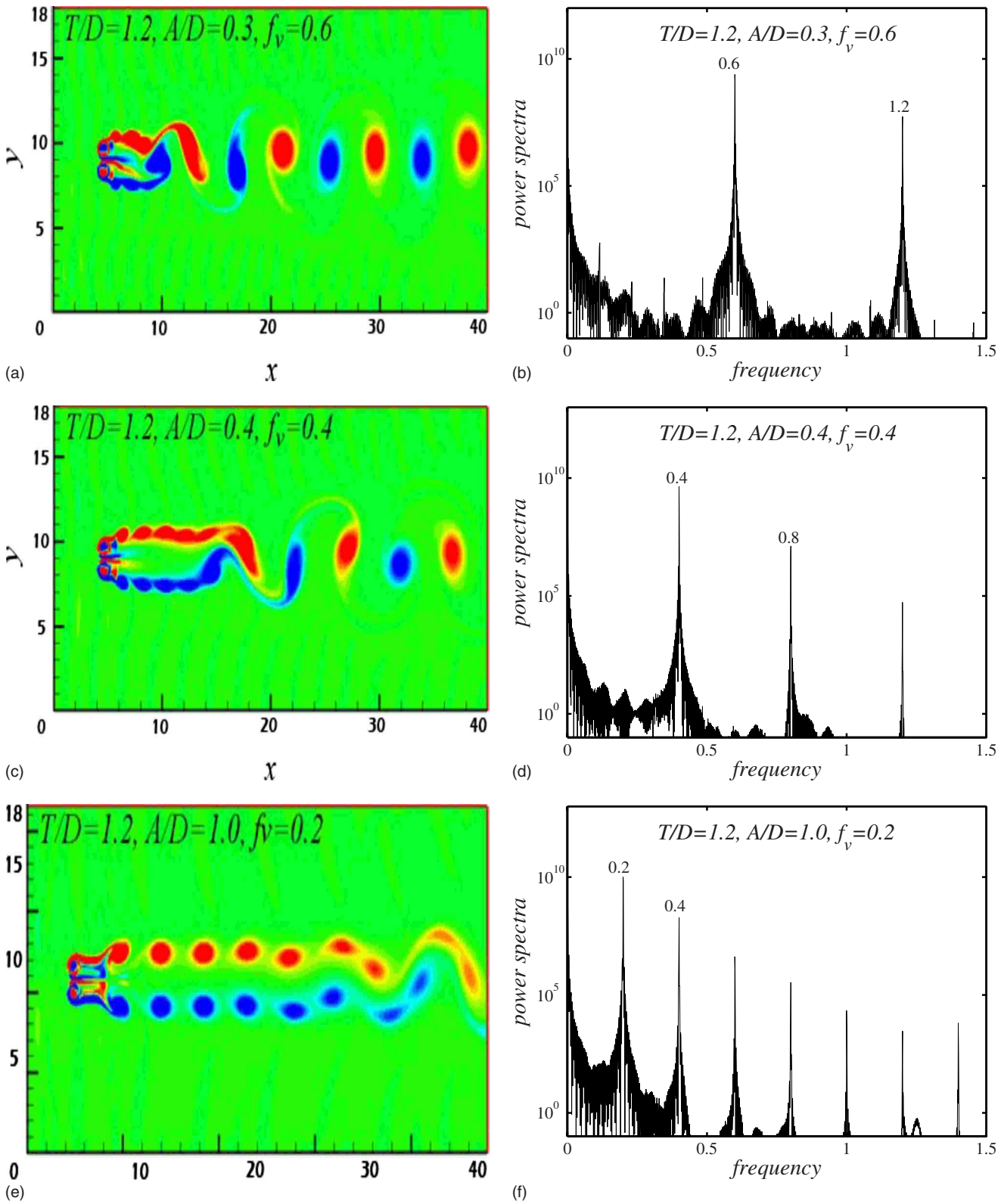

FIG. 10. (Color online) Vortex formation and lift power spectral analysis for vibrating cylinders at $T/D=1.2$.

quency is the same as the cylinder vibration frequency.

From the discussion of Figs. 4–7, it can be seen that, for $f_v=0.4$, there exists a threshold of vibration amplitude; when the vibration amplitude is larger than this threshold, then the vortex shedding is completely locked up by the cylinder vibration frequency f_v. Here, the term "completely locked up" indicates that the cylinder vibration frequency f_v completely suppresses the original vortex shedding frequency in the spectral analysis. The most distinct vortex lock-up phenomenon occurs at $T/D=1.2$ and 1.6. To further investigate the

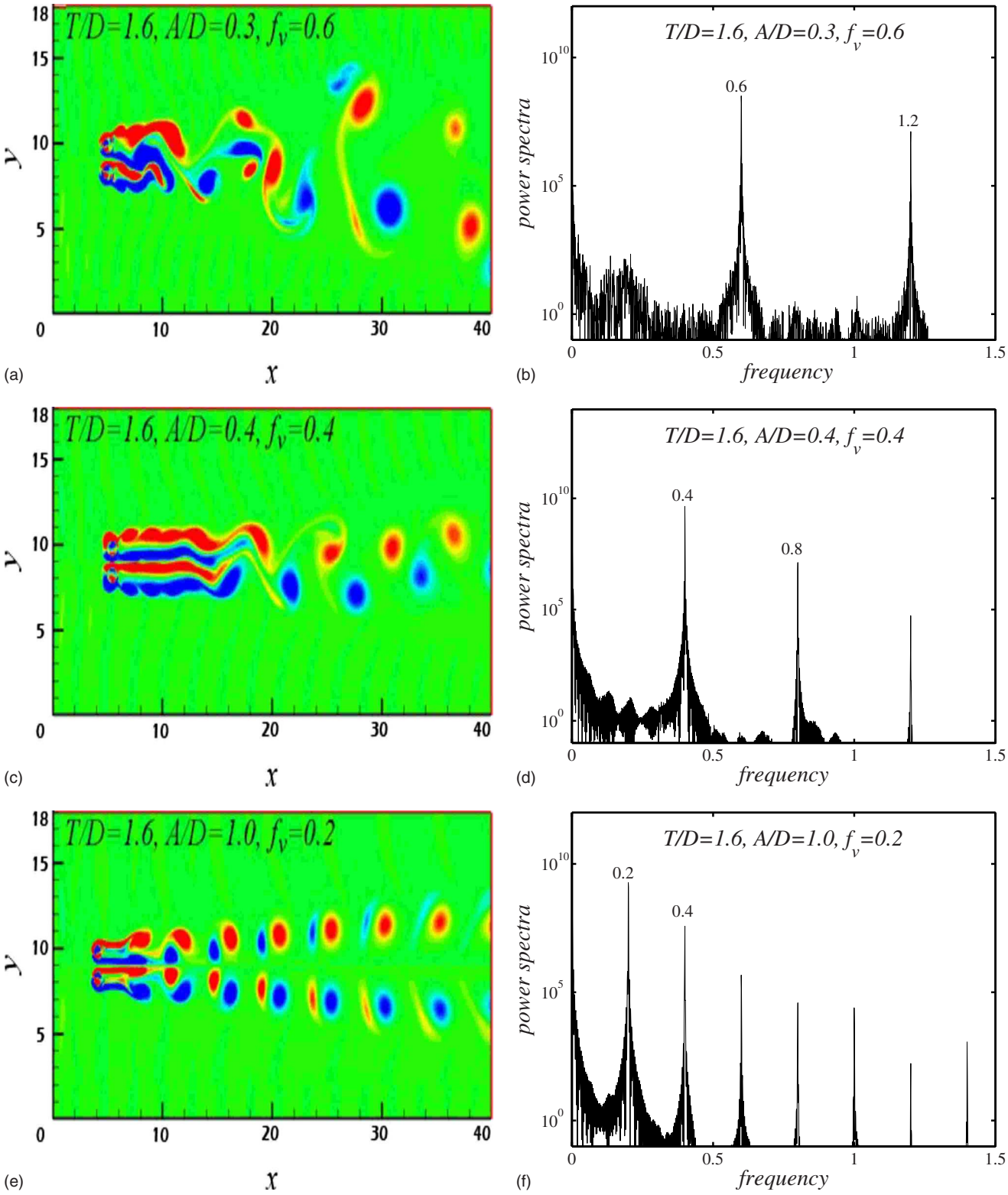

FIG. 11. (Color online) Vortex formation and lift power spectral analysis for vibrating cylinders at $T/D=1.6$.

effect of vibration frequency and amplitude on vortex lockup, we examined the vortex formation at vibration frequency $f_v=0.2$, 0.4, and 0.6, respectively. Figure 10 shows, at $T/D=1.2$, the vortex lock-up phenomenon, and their spectral analysis at different cylinder vibration frequencies and amplitudes. At $f_v=0.6$, the vortex shedding is locked up when the vibration amplitude $A/D=0.3$, i.e., the vortex shedding frequency is dominated by $f_v=0.6$, which is evidenced by the spectral analysis. At $f_v=0.4$, this vortex lock-up amplitude becomes $A/D=0.4$; with further decrease in the vibration frequency to $f_v=0.2$, the vortex lock-up amplitude increases to $A/D=1.0$. A similar phenomenon can be found

for $T/D=1.6$, as shown in Fig. 11. From these discussions, it can be concluded that, with lower vibration frequency, the threshold of the vibration amplitude should be big enough to capture the vortex lock-up phenomenon.

V. CONCLUSIONS

In the present study, a 2D fluid-structure interaction problem for two side-by-side cylinders vibrating in a cross flow has been simulated using MRTLBM. A moving boundary scheme is applied to accommodate the vibration of the cylinders. Calculations were carried out for four spacing ratios at Re=200. The present calculations limit T/D to those values that would not allow the cylinders to touch each other, even under the most severe vibration. In order to establish the credibility of the present numerical method, a thorough comparison of the rigid case is made with previously reported lift and drag calculations and their associated frequencies, and flow visualization results. The following conclusions can be drawn from the calculations.

(1) The current numerical technique can reproduce the same phenomena observed in the experiments reported by Williamson [9], such as the flow patterns at different T/D. This lends further credence to the mechanism of vortex formation reported in the rigid case.

(2) The vibration of cylinders has a significant influence on the vortex formation in the near wake. Particularly for $T/D=1.2$ and 1.6, the cylinder vibration can regulate the vortex shedding into regular patterns.

(3) The vortex shedding from the two cylinders can be locked up by the vibration of the cylinder pair. There exists a threshold for the vortex lock-up phenomenon. With increasing cylinder vibration frequency, the threshold of the vibration amplitude for the lock-up phenomenon decreases.

(4) The proposed multiple relaxation time lattice Boltzmann method can be used effectively to resolve the flow-induced vibration behavior in the case of two side-by-side cylinders. This means that the technique could be extended to similar problems with multiple structures.

ACKNOWLEDGMENTS

Funding support given by the Research Grants Council of the Government of the HKSAR under Grant No. 5221/05E, the National Natural Science Foundation of China under Grant No. 10572130, the National Basic Research Programs of China under grant No. 2006CB708612, and the Natural Science Foundation of Zhejiang Province under Grant No. Y607425 is gratefully acknowledged.

[1] S. S Chen, J. C. Simonis and Y.S. Shin, in *Flow-Induced Vibration—1986*, Proceedings of ASME Pressure Vessel and Piping Conference and Exhibit, Chicago, Illinois, 1986, edited, by S. S. Chen, J. C. Simonis, and Y. S. Shin (ASME, New York, 1986) Vol. 104, pg. 221.
[2] H. J. Kim, J. Fluid Mech. **196**, 431 (1988).
[3] T. Farrant, M. Tan, and W. G. Price, Comput. Fluids **30**, 211 (2001).
[4] J. R. Meneghini *et al.*, J. Fluids Struct. **15**, 327 (2001).
[5] S. Kang, Phys. Fluids **15**, 2486 (2003).
[6] W. Jester and Y. Kallinderis, J. Fluids Struct. **17**, 561 (2003).
[7] H. M. Spivack, J. Aerosol Sci. **13**, 289 (1946).
[8] P. W. Bearman and A. J. Wadcock, J. Fluid Mech. **61**, 499 (1973).
[9] C. Williamson, J. Fluid Mech. **159**, 1 (1985).
[10] D. Sumner, S. S. T. Wang, S. J. Price and M. P. Paidoussis, J. Fluids Struct **13**, 309–338 (1999).
[11] P. K. Stansby, Aeronaut. Q. **32**, 48 (1981).
[12] K. Chang and C. Song, Int. J. Numer. Methods Fluids **11**, 317 (1990).
[13] S. Mittal, V. Kumar, and A. Raghuvanshi, Int. J. Numer. Methods Fluids **25**, 1315 (1997).
[14] K. Schulz and Y. Kallinderis, Offshore Technology Conference Technical Report OTC 8699, 1998 (unpublished).
[15] T. E. Tezduyar *et al.*, Int. J. Numer. Methods Fluids **11**, 515 (1990).
[16] A. Slaouti and P. K. Stansby, J. Fluids Struct. **6**, 641 (1992).
[17] M. M. Zdravkovich, J. Fluids Struct. **1**, 239 (1987).
[18] C. Norberg, J. Fluids Struct. **17**, 57 (2003).
[19] C. Evangelinos and G. E. Karniadakis, J. Fluid Mech. **400**, 91 (1999).
[20] J. C. R. Hunt, Proc. Inst. Mech. Eng. **209**, 297 (1995).
[21] H. Chen, S. Chen, and W. H. Matthaeus, Phys. Rev. A **45**, R5339 (1992).
[22] Y. Qian, D. d'Humières, and P. Lallemand, Europhys. Lett. **17**, 479 (1992).
[23] P. Lallemand and L. S. Luo, Phys. Rev. E **61**, 6546 (2000).
[24] X. He and L. S Luo, Phys. Rev. E **56**, 6811 (1997).
[25] R. Surmas *et al.*, Future Gener. Comput. Syst. **20**, 951 (2004).
[26] H. Fang, Z. Lin, and Z. Wang, Phys. Rev. E **57**, R25 (1998).
[27] Y. Liu, Comput. Fluids **37**, 724 (2008).
[28] Y. S. Xu, Y. Liu, X. Z. Xu, and G. X. Huang, J. Electrochem. Soc. **153**, A607 (2006).
[29] Y. Liu, R. M. C. So, Y. L. Lau, and Y. Zhou, J. Fluids Struct. **15**, 1009 (2001).
[30] Y. Liu, R. M. C. So, and Z. X. Cui, J. Fluids Struct. **20**, 589 (2005).
[31] Y. Liu and Z. X. Cui, Int. J. Comput. Fluid Dyn. **20**, 379 (2006).
[32] Y. Liu, R. M. C. So, and Z. X. Cui, Comput. Fluids **35**, 951 (2006).
[33] R. M. C. So, Y. Liu, Z. X. Cui, C. H. Zhang, and X. Q. Wang, J. Fluids Struct. **20**, 373 (2005).
[34] D. d'Humières, Prog. Astronaut. Aeronaut. **159**, 450 (1992).
[35] I. Ginzburg, Adv. Water Resour. **28**, 1171 (2005).
[36] D. d'Humières, I. Ginzburg, M. Krafczyk, P. Lallemand, and L. S. Luo, Philos. Trans. R. Soc. London, Ser. A **360**, 437 (2002).
[37] P. Lallemand and L. S. Luo, J. Comput. Phys. **184**, 406 (2003).
[38] L. S. Luo, Phys. Rev. Lett. **81**, 1618 (1998).
[39] L. S. Luo, Phys. Rev. E **62**, 4982 (2000).
[40] M. Griffin and S. E. Ramberg, J. Fluid Mech. **75**, 257 (1976).